Large-Scale Photonic Ising Machine by Spatial Light Modulation

D. Pierangeli,[1,2,*] G. Marcucci,[1,2] and C. Conti[1,2]

[1]*Dipartimento di Fisica, Università di Roma "La Sapienza," P.le Aldo Moro 5, 00185 Rome, Italy*
[2]*Institute for Complex Systems, National Research Council (ISC-CNR), Via dei Taurini 19, 00185 Rome, Italy*

Quantum and classical physics can be used for mathematical computations that are hard to tackle by conventional electronics. Very recently, optical Ising machines have been demonstrated for computing the minima of spin Hamiltonians, paving the way to new ultrafast hardware for machine learning. However, the proposed systems are either tricky to scale or involve a limited number of spins. We design and experimentally demonstrate a large-scale optical Ising machine based on a simple setup with a spatial light modulator. By encoding the spin variables in a binary phase modulation of the field, we show that light propagation can be tailored to minimize an Ising Hamiltonian with spin couplings set by input amplitude modulation and a feedback scheme. We realize configurations with thousands of spins that settle in the ground state in a low-temperature ferromagneticlike phase with all-to-all and tunable pairwise interactions. Our results open the route to classical and quantum photonic Ising machines that exploit light spatial degrees of freedom for parallel processing of a vast number of spins with programmable couplings.

A large number of internal states characterize complex systems from biology to social science. The fact that the number of these states grows exponentially with the system size hampers large-scale computational possibilities. Complex optimization problems involving these models are in many cases classified as nondeterministic polynomial (NP) hard and cannot be tackled efficiently by standard computing architectures. A broad class of such computationally intractable problems maps to the search of the ground state of a classical system of interacting spins: the minimization of an Ising Hamiltonian with specific spin couplings [1–3].

Growing research interest is emerging towards physical and artificial systems that evolve according to an Ising Hamiltonian and enable us to find the optimal combinatorial solution by the ground state observed in the experiment. Quantum and classical Ising systems have been realized by trapped atoms [4,5], single photons [6], superconducting circuits [7], electromechanical modes [8], nanomagnets [9] and polariton condensates [10]. In optics, spin-glass dynamics have been observed in random lasers [11,12], multimodal cavities [13,14], coupled laser lattices [15], beam filamentation [16], and nonlinear wave propagation in disordered media [17]. These photonic systems host thousands of optical spins, but the spin variables are not easy to access, and controlling their interaction is challenging.

Novel photonic platforms with numerous and easily accessible spins are particularly relevant for computation. Optical computing machines offer high-speed and parallelization. Various authors reported coherent Ising machines based on time-multiplexed optical parametric oscillators finding approximate solutions to optimization problems with several nodes [18–24]. Others proposed nanophotonic circuits to implement any small-scale spin systems directly on a programmable chip [25–27]. Matrix operations can also be performed by spatially shaped optical fields, without engineered wave-mixing devices [28,29], by exploiting randomly reflected waves [30] or disordered biological samples [31]. However, using spatial optical modulation to solve Ising spin dynamics has remained unexplored.

In this Letter, we propose and experimentally demonstrate the use of spatial light modulation for calculating the ground state of an Ising Hamiltonian. The phase matrix on a spatial light modulator (SLM) acts as a lattice of spins for which the interaction is ruled by the constrained optical intensity in the far field and can be programmed by input amplitude modulation. Feedback from the detection plane allows the spatial phase distribution to evolve towards the minimum of the selected spin model. We find ferromagneticlike ground states in agreement with mean-field predictions. Our spatial Ising machine hosts thousands of parallelly processed spins, and it represents a scalable and efficient approach for photonic computing.

We implement a spatial photonic Ising machine by using the phases in separated spatial points of the optical wave front. A binary phase-modulated beam encodes binary spins with configurable interactions [Fig. 1(a)]. A spin variable $\sigma_j = \exp(\iota\phi_j) = \pm 1$ corresponds to a spatial point of the optical field with phase $\phi_j \in \{0, \pi\}$. As illustrated in Figs. 1(b) and 1(c), a SLM acting as a reprogrammable matrix of pixels imprints binary phase values on the coherent wave front. Setting the SLM in the Fourier space of the electric field $\tilde{E}(k)$, we have
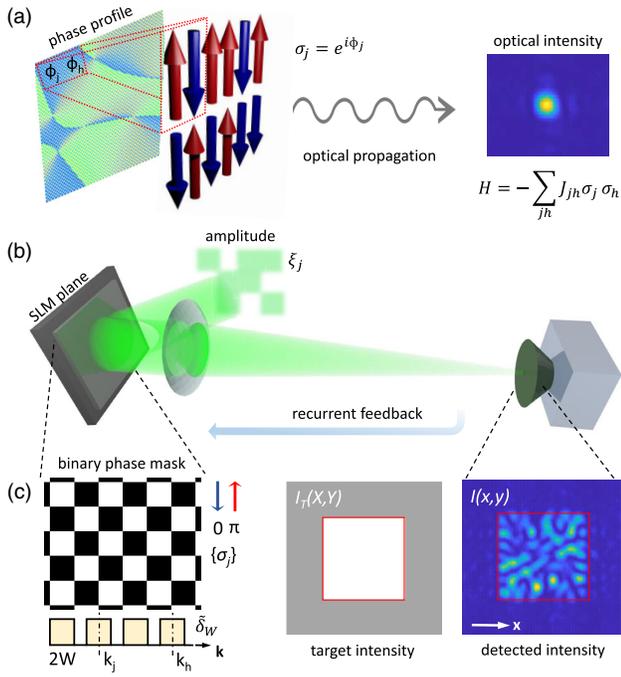
FIG. 1. Ising machine by spatial light modulation. (a) The wave phase in different spatial points gives the spins evolving through optical propagation. (b) An amplitude-modulated laser beam is phase modulated by a reflective SLM and detected by a CCD camera in the far field. (c) A discrete phase mask with binary values $\phi_j = 0, \pi$ in the Fourier plane mimics Ising spins $\sigma_j = \pm 1$. Inset is an example of the detected intensity when the binary hologram is tailored to generate a squared intensity target I_T.

$$\tilde{E}(k) = \sum_j \xi_j \sigma_j \tilde{\delta}_W(k - k_j), \qquad (1)$$

where ξ_j indicates the field amplitude incoming on each pixel. The normalized rectangular function $\tilde{\delta}_W$ models the pixel of finite size $2W$ [Fig. 1(c)] so that $k_j = 2Wj$, with $j = 1, \ldots, n$. The resulting far-field intensity after free-space propagation is

$$I(x) = |E(x)|^2 = \sum_{jh} \xi_j \xi_h \sigma_j \sigma_h \delta_W^2(x) e^{2\imath W(h-j)x}, \quad (2)$$

with $\delta_W(x) = \sin(Wx)/(Wx)$ as the inverse Fourier transform of $\tilde{\delta}_W(k)$. A spin-spin interaction can be induced by acting on the intensity on the detection plane. We constrain $I(x)$ by a measurement and feedback method to couple the phases on the SLM plane. Minimizing $\|I_T(x) - I(x)\|$ for an arbitrary target intensity image $I_T(x)$ thus corresponds to minimizing a Hamiltonian H. After normalization, $\int [I_T(x)]^2 dx \simeq \int [I(x)]^2 dx$, and the function H takes the form of the Ising Hamiltonian

$$H = -\sum_{jh} J_{jh} \sigma_j \sigma_h, \qquad (3)$$

with spin interactions given by

$$J_{jh} = 2\xi_j \xi_h \int I_T(x) \delta_W^2(x) e^{2\imath W(h-j)x} dx. \qquad (4)$$

When the effect of the SLM pixel size can be neglected, $\delta_W(x) \sim 1$, and the couplings reduce to

$$J_{jh} = 2\pi \xi_j \xi_h \tilde{I}_T[2W(j - h)], \qquad (5)$$

which indicates that the interaction matrix is set by the input amplitude modulation along with the Fourier transform of the far-field target image. The interaction passes from short to long range by changing the spatial profile of I_T. In particular, in the case of a pointlike target image, the spins are all-to-all interacting ($J_{jh} = $ const) for an input wave with constant amplitude. Using a programmable (quenched) amplitude mask on the input beam, the couplings can be varied according to $J_{jh} \propto \xi_j \xi_h$, which allows us to implement the entire class of spin-glass models, known as Mattis models [32,33], where the pairwise interaction can be expressed as a product of two independent variables. Figure 1(c) shows the principle of operation of our Ising machine. A spin configuration $\{\sigma_j\}$ is generated upon an amplitude-modulated wave front using binary phases on the SLM, and the corresponding intensity distribution $I(x)$ is measured in the far field. The detected image is compared with the target $I_T(x)$ and the information is feedback to the SLM plane. The system evolves towards minimization of the cost function $f = \|I_T(x) - I(x)\|$, which corresponds to the Ising ground state.

The experimental optical machine follows the setting shown in Fig. 1(b). Light from a continuous-wave laser source with a wavelength of $\lambda = 532$ nm is expanded, eventually modulated in amplitude, and impinges on a nematic liquid crystal reflective modulator (Holoeye LC-R 720, 1280×768 pixels, with pixel pitch of 20×20 μm) for which the active area is selected by a rectangular aperture to host $N = L \times L$ spins (in pixels). The SLM is set into a phase-modulation mode with less than 10% residual intensity modulation by a combination of incident and analyzed polarizations. Phase-modulated light is spatially filtered (3 mW of power) and then focused by a lens ($f = 500$ mm) on a CCD camera. The intensity is measured on $M = 18 \times 18$ spatial modes obtained by grouping 16×16 camera pixels to average over speckles arising from spatial phase fluctuations in the far-field plane.

We first demonstrate the spatial Ising machine for $N = 4 \times 10^4$ spins with all-to-all couplings ($J_{jh} = $ const), which corresponds to a number of spin-spin connections that are orders of magnitude larger than those realized in time-multiplexed platforms [19,20]. In this case, $\xi_j = \xi_h = \xi_0$ and the target corresponds to intensity focused only in a single spatial mode: a bright localized spot [Fig. 2(a)]. The binary phases on the SLM are initialized
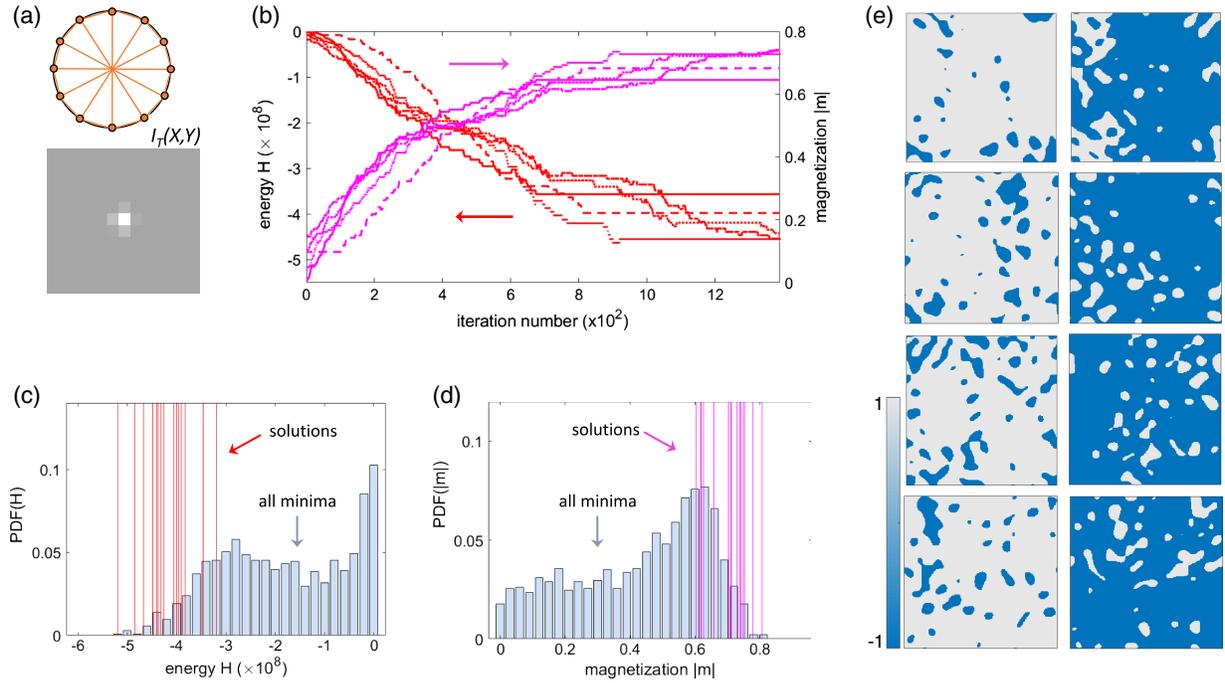
FIG. 2. Optically solving the Ising Hamiltonian with all-to-all spin interactions. (a) Unweighted Möbius-Ladder graph with fully connected vertices (results refer to $N = 4 \times 10^4$) along with the target intensity I_T. (b) Measured evolution of H ($J_{jh} = 1$) and $|m|$ for different initial random spin matrices. (c),(d) Observed probability distribution for the (c) energy and (d) magnetization of spin configurations satisfying the interaction constraint I_T; red and magenta lines indicate H and $|m|$ of the identified ground-state solutions, respectively. (e) Set of ground-state spin configurations: small-size ferromagnetic clusters with opposite magnetization are visible.

by a random distribution, which gives a weak and broad speckle pattern in the detection plane. By a Monte-Carlo-like method, at each iteration, we randomly flip a small cluster of spins and measure the corresponding far-field intensity, retaining the change only if its difference with the target image decreases [34]. Unlike other photonic Ising machines [23], no information about the target Hamiltonian is used to electronically affect the spin evolution. To prevent trapping into local minima induced by the algorithm, we select clusters with a gradually increasing size. To follow the system evolution, we consider as physical observables the energy H and the magnetization $m = \langle \sigma_j \rangle$ of each configuration. As shown in Fig. 2(b) for different realizations, we observe a monotonic growth of $|m|$, which saturates to a large value after approximatively 10^3 iterations. The Hamiltonian monotonically decreases toward a plateau, thus indicating the onset of a low-energy ferromagneticlike state. The actual temperature T of these spin configurations is determined by the random phase fluctuations in the Fourier plane, which results from the intrinsic noise characterizing each operation in the experimental setup. Sources of noise come from the quantization on the CCD discrete modes of the detected intensity, as well as from the imperfect spatial phase modulation [35].

To test the solution found by our machine, we use a different approach based on phase retrieval. The aim is to evaluate the energy probability distribution function (PDF) of all those $\{\sigma_j\}$ that satisfy the far-field constraint and compare with the low-energy solutions found by the machine. We use a quantized phase-retrieval (QPR) algorithm [36] to generate binary phase distributions from the target image I_T and measure the far-field intensity I. Among the many QPR states, which are associated with different phase patterns in the target plane, the solution of the machine is determined by minimizing the cost function f. Figures 2(c) and 2(d) show the results from 16 sets of measurements, each with 100 phase-retrieved spin configurations. The identified solutions populate the tail of the energy distribution [Fig. 2(c)] and have maximum magnetization [Fig. 2(d)]. This indicates that ground states of the Ising Hamiltonian are successfully found. In particular, the machine gives, with 87% probability, the correct minimum solution: that is, a spin configuration lying in 5% of those with the lowest energy. This ground-state probability quantifies the correspondence between the cost-function minima and spin states with lower energy, and it is independent of the way the ground state has been found.

To quantify the physical state resulting from the optical computation, we analyze the spin configurations. Figure 2(e) shows the typical ground states retrieved by the optical machine. We observe ferromagnetic domains of various size embedded in a phase with opposite magnetization. Spin states with $m < 0$ and $m > 0$ appear with

almost equal probability, as expected from spontaneous symmetry breaking in the absence of external magnetic fields. From the set of $\{\sigma_j\}$, we estimate the actual temperature according to the mean-field solution of Eq. (3), which describes the case with all-to-all interacting spins [33,37]. Considering the equation of state $m = \tanh\left[(T_c/T)m\right]$, from the observed mean magnetization, we obtain $T/T_c = 0.80 \pm 0.03$. We also analyze the measured spin spatial autocorrelation according to $g(r) = \exp\left(-r/\xi\right)$, where the autocorrelation length ξ estimates the mean domain size. In the mean-field approach, ξ diverges at the critical temperature as $\xi = R_*(1 - T/T_c)^{-\beta}$, where the critical exponent is $\beta = 1/2$ and R_* is the minimum cluster length. The resulting temperature is $T/T_c = 0.83 \pm 0.02$. Therefore, the observed ground states have magnetizations and domain configurations consistent with a mean-field Ising model at fixed temperature.
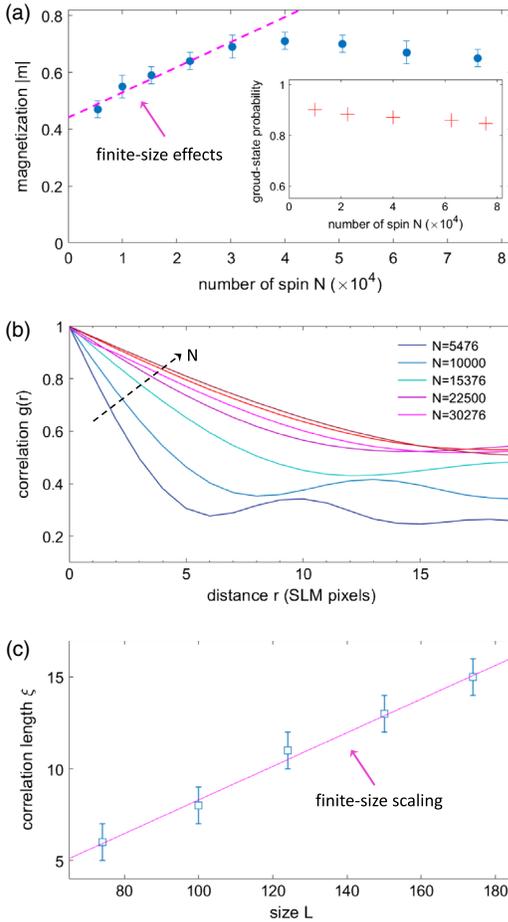
FIG. 3. Scaling properties of the ferromagnetic ground state. (a) Observed magnetization varying the spin number. The inset shows the scaling of the machine performance. (b) Spatial spin autocorrelation functions (distance in pixel units) for different N. (c) Autocorrelation length as a function of the system size L (dots) and linear fitting behavior (line).

One of the main features of our spatial photonic setting is the extremely large number of spins that can be simulated. Varying the active area on the SLM (the transverse size of the spatially modulated laser beam), we investigate how the machine operation depends on the system size L. Figure 3(a) shows the magnetization and the fidelity (probability of finding the Ising ground state) of the observed ground state by varying the number of spins from $N = 74 \times 74$ to $N = 274 \times 274$ and leaving their interaction unchanged. At variance with other photonic settings [19], we find that the performance of our Ising machine does not sensibly depend on the number of spins [inset in Fig. 3(a)]. For large sizes N, a minor decrease of the magnetization and fidelity is observed, and it is due to the lower spatial resolution in the detection plane. At a low spin number, we observe a linear decrease of $|m|$ as N is reduced. We ascribe this behavior to finite-size effects. The observed spin autocorrelation function strongly varies with the number of spins, and a well-defined single decay only emerges at large N [Fig. 3(b)]. For configurations with few spins, we find that the measured correlation length grows linearly with the configuration size [Fig. 3(c)], which is in agreement with finite-size scaling arguments, which predict a mean-field behavior of $\xi \propto L$ [38]. For large L, the size of the ferroelectric domains becomes independent of the system scale. The photonic machine thus points out a fundamental phenomenon of spin models [39].

We investigate other Ising models by tailoring the spin couplings. As suggested by Eq. (5), Mattis spin glasses can be realized by varying the input amplitudes ξ_i and keeping a pointlike target image ($\tilde{I}_T[2W(i - j)] \simeq \text{const}$). For these experiments, the SLM is split into two independent parts [40]. A portion of the SLM is used for amplitude
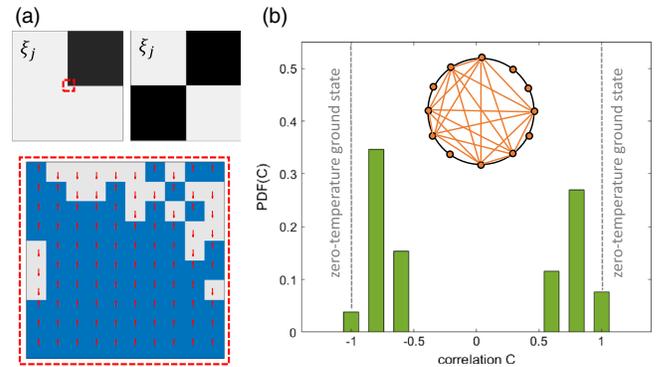
FIG. 4. Programming the spin interaction by amplitude modulation. (a) Examples of coupling configurations ($N = 10^4$, top panels) made of random blocks in which the interaction assumes two positive values ($\xi_j = 0, \xi_0 > 0$). The corresponding spin ground state observed in the red box region is shown in the bottom panel. (b) Measured probability distribution of the correlation C between the ground state and the couplings for the Mattis models. The inset shows a corresponding Möbius-Ladder graph with connected and unconnected nodes.

modulation to generate controlled ξ_i distributions that are imaged pixel by pixel on the second portion, where binary phase modulation and spin dynamics occur. We implement coupling matrices $J_{jh} \propto \xi_j \xi_h$ made of large random blocks with strongly ($\xi_j = \xi_0$) and weakly ($\xi_j = 0$) interacting spins [Fig. 4(a)]. Following the theoretical solution of the Mattis model [33], the expected spin ground state is identical to the interaction configuration ξ_j or to its reversal, except for the weakly interacting regions where spins are randomly oriented. In our photonic simulation, we quantify the fidelity of the measured inhomogeneous ferromagnetic ground state by the spatial correlation $C = \sum_j \sigma_j \xi_j / \xi_0$. $C = \pm 1$ for the ideal Mattis model in the lowest energy state. Figure 4(b) shows that the measured ground states are strongly correlated or anticorrelated with the interaction matrix, as expected. Because, in the Mattis models, a minimal amount of noise introduces frustration [33], the differences between the machine solutions and the ideal ones are due to the non-zero effective temperature of the system.

In conclusion, we have demonstrated that spatial light modulation can be exploited to find the ground state of Ising Hamiltonians. By using binary phases on the wave front of an amplitude-modulated laser beam and a detection and feedback method, we optically calculate the low-energy ferromagnetic spin configuration. The ground states display finite-size scaling effects and mean-field properties at a fixed temperature. This finding opens the way to photonic simulations of phase-transition phenomena. The platform naturally hosts tens of thousands of spins (not limited to binary spins, when adopting multilevel phase modulations) and is scalable to larger sizes. The speed of our machine is limited only by the SLM response, camera rate, and data processing. The iteration time can be potentially reduced to a few milliseconds with the most recent technologies [41]. Moreover, a recent theoretical proposal for optical circuits [27] suggests a possible direction for further reducing the steps performed digitally using wave-mixing devices. Our method, employing fast and low-loss optical computation, may also find application in alleviating energy-consuming operations in electronics as large matrix multiplications and Fourier transforms. Our approach can be extended to light pulses modulated in space and time, even including the quantum optical regimes in which the coherent laser source is replaced by nonclassical light. Similar large-scale simulators may also be conceived with quantum wave packets as in ultracold gases, and Bose-Einstein condensates, by proper control and preparation of the initial states.

---

[*]Davide.Pierangeli@roma1.infn.it

[1] F. Barahona, On the computational complexity of Ising spin glass models, J. Phys. A **15**, 3241 (1982).

[2] A. Lucas, Ising formulations of many NP problems, Front. Phys. **2**, 1 (2014).

[3] G. De las Cuevas and T. S. Cubitt, Simple universal models capture all classical spin physics, Science **351**, 1180 (2016).

[4] K. Kim, M.-S. Chang, S. Korenblit, R. Islam, E. E. Edwards, J. K. Freericks, G.-D. Lin, L.-M. Duan, and C. Monroe, Quantum simulation of frustrated Ising spins with trapped ions, Nature (London) **465**, 590 (2010).

[5] J. W. Britton, B. C. Sawyer, A. C. Keith, C.-C. J. Wang, J. K. Freericks, H. Uys, M. J. Biercuk, and J. J. Bollinger, Engineered two-dimensional Ising interactions in a trapped-ion quantum simulator with hundreds of spins, Nature (London) **484**, 489 (2012).

[6] X. Ma, B. Dakic, W. Naylor, A. Zeilinger, and P. Walther, Quantum simulation of the wavefunction to probe frustrated Heisenberg spin systems, Nat. Phys. **7**, 399 (2011).

[7] M. W. Johnson *et al.*, Quantum annealing with manufactured spins, Nature (London) **473**, 194 (2011).

[8] I. Mahboob, H. Okamoto, and H. Yamaguchi, An electromechanical Ising Hamiltonian, Sci. Adv. **2**, e1600236 (2016).

[9] B. Sutton, K. Y. Camsari, B. Behin-Aein, and S. Datta, Intrinsic optimization using stochastic nanomagnets, Sci. Rep. **7**, 44370 (2017).

[10] N. G. Berloff, M. Silva, K. Kalinin, A. Askitopoulos, J. D. Topfer, P. Cilibrizzi, W. Langbein, and P. G. Lagoudakis, Realizing the classical XY Hamiltonian in polariton simulators, Nat. Mater. **16**, 1120 (2017).

[11] N. Ghofraniha, I. Viola, F. Di Maria, G. Barbarella, G. Gigli, L. Leuzzi, and C. Conti, Experimental evidence of replica symmetry breaking in random lasers, Nat. Commun. **6**, 6058 (2015).

[12] F. Tommasi, E. Ignesti, S. Lepri, and S. Cavalieri, Robustness of replica symmetry breaking phenomenology in random laser, Sci. Rep. **6**, 37113 (2016).

[13] A. L. Moura, P. I. R. Pincheira, A. S. Reyna, E. P. Raposo, A. S. L. Gomes, and C. B. de Arajo, Replica Symmetry Breaking in the Photonic Ferromagneticlike Spontaneous Mode-Locking Phase of a Multimode Nd:YAG Laser, Phys. Rev. Lett. **119**, 163902 (2017).

[14] S. Basak, A. Blanco, and C. Lopez, Large fluctuations at the lasing threshold of solid- and liquid-state dye lasers, Sci. Rep. **6**, 32134 (2016).

[15] M. Nixon, E. Ronen, A. A. Friesem, and N. Davidson, Observing Geometric Frustration with Thousands of Coupled Lasers, Phys. Rev. Lett. **110**, 184102 (2013).

[16] W. Ettoumi, J. Kasparian, and J.-P. Wolf, Laser Filamentation as a New Phase Transition Universality Class, Phys. Rev. Lett. **114**, 063903 (2015).

[17] D. Pierangeli, A. Tavani, F. Di Mei, A. J. Agranat, C. Conti, and E. DelRe, Observation of replica symmetry breaking in disordered nonlinear wave propagation, Nat. Commun. **8**, 1501 (2017).

[18] A. Marandi, Z. Wang, K. Takata, R. L. Byer, and Y. Yamamoto, Network of time-multiplexed optical parametric oscillators as coherent Ising machine, Nat. Photonics **8**, 937 (2014).

[19] P. L. McMahon *et al.*, A fully-programmable 100-spin coherent Ising machine with all-to-all connections, Science **354**, 614 (2016).

[20] T. Inagaki *et al.*, A coherent Ising machine for 2000-node optimization problems, Science **354**, 603(R) (2016).

[21] T. Inagaki, K. Inaba, R. Hamerly, K. Inoue, Y. Yamamoto, and H. Takesue, Large-scale Ising spin network based on degenerate optical parametric oscillators, Nat. Photonics **10**, 415 (2016).

[22] Y. Takeda, S. Tamate, Y. Yamamoto, H. Takesue, T. Inagaki, and S. Utsunomiya, Boltzmann sampling for an XY model using a non-degenerate optical parametric oscillator network, Quantum Sci. Technol. **3**, 014004 (2018).

[23] A. D. King, W. Bernoudy, J. King, A. J. Berkley, and T. Lanting, Emulating the coherent Ising machine with a mean-field algorithm, arXiv:1806.08422v1.

[24] L. Bello, M. C. Strinati, E. G. Dalla Torre, and A. Pe'er, Dynamics of coupled parametric oscillators beyond coupled Ising spins, arXiv:1901.06202v2.

[25] Y. Shen *et al.*, Deep learning with coherent nanophotonic circuits, Nat. Photonics **11**, 441 (2017).

[26] N. C. Harris *et al.*, Quantum transport simulations in a programmable nanophotonic processor, Nat. Photonics **11**, 447 (2017).

[27] C. Roques-Carmes *et al.*, Photonic recurrent Ising sampler, arXiv:1811.02705v1.

[28] S. R. Huisman, T. J. Huisman, T. A. W. Wolterink, A. P. Mosk, and P. W. H. Pinkse, Programmable multiport optical circuits in opaque scattering materials, Opt. Express **23**, 3102 (2015).

[29] R. Fickler, M. Ginoya, and R. W. Boyd, Custom-tailored spatial mode sorting by controlled random scattering, Phys. Rev. B **95**, 161108(R) (2017).

[30] P. del Hougne and G. Lerosey, Leveraging Chaos for Wave-Based Analog Computation: Demonstration with Indoor Wireless Communication Signals, Phys. Rev. X **8**, 041037 (2018).

[31] D. Pierangeli, V. Palmieri, G. Marcucci, C. Moriconi, G. Perini, M. De Spirito, M. Papi, and C. Conti, Deep optical neural network by living tumour brain cells, arXiv:1812 .09311.

[32] D. C. Mattis, Solvable spin systems with random inter-actions, Phys. Lett. A **56**, 421 (1976).

[33] H. Nishimori, *Statistical Physics of Spin Glasses and Information Processing: An Introduction* (Clarendon, Oxford, 2001), Vol. 111.

[34] I. M. Vellekoop and A. P. Mosk, Phase control algorithms for focusing light through turbid media, Opt. Commun. **281**, 3071 (2008).

[35] A. Jesacher, A. Schwaighofer, S. Furhapter, C. Maurer, S. Bernet, and M. Ritsch-Marte, Wavefront correction of spatial light modulators using an optical vortex image, Opt. Express **15**, 5801 (2007).

[36] F. Wyrowski, Diffractive optical elements: Iterative calcu-lation of quantized, blazed phase structures, J. Opt. Soc. Am. A **7**, 961 (1990).

[37] G. Parisi, *Statistical Field Theory*, Frontiers in Physics 66 (Addison-Wesley, Reading, MA, 1988).

[38] D. P. Landau, Finite-size behavior of the Ising square lattice, Phys. Rev. B **13**, 2997 (1976).

[39] K. Binder and D. W. Heermann, *Monte Carlo Simulation in Statistical Physics* (Springer-Verlag, Berlin, 1997).

[40] A. Jesacher, C. Maurer, A. Schwaighofer, S. Bernet, and M. Ritsch-Marte, Near-perfect hologram reconstruction with a spatial light modulator, Opt. Express **16**, 2597 (2008).

[41] Y. Liu, C. Ma, Y. Shen, J. Shi, and L. V. Wang, Focusing light inside dynamic scattering media with millisecond digital optical phase conjugation, Optica **4**, 280 (2017).